Tuning of Adsorption and Magnetic Properties in a Series of Self-Templated Isostructural Ni(II) Metal-Organic Frameworks

ARTICLE *in* CRYSTAL GROWTH & DESIGN · FEBRUARY 2014

Impact Factor: 4.89 · DOI: 10.1021/cg401590w

6 AUTHORS, INCLUDING:

Miguel Cortijo
Centre d'Élaboration de Matériaux et d'Etudes…
7 PUBLICATIONS **28** CITATIONS
SEE PROFILE

Santiago Herrero
Complutense University of Madrid
42 PUBLICATIONS **420** CITATIONS
SEE PROFILE

Reyes Jimenez-Aparicio
Complutense University of Madrid
100 PUBLICATIONS **1,574** CITATIONS
SEE PROFILE

Josefina Perles
Complutense University of Madrid
51 PUBLICATIONS **597** CITATIONS
SEE PROFILE

CRYSTAL GROWTH & DESIGN

Article

pubs.acs.org/crystal

Tuning of Adsorption and Magnetic Properties in a Series of Self-Templated Isostructural Ni(II) Metal−Organic Frameworks

Miguel Cortijo, Santiago Herrero,* Reyes Jiménez-Aparicio,* Josefina Perles, José L. Priego, and Javier Torroba

Departamento de Química Inorgánica, Facultad de Ciencias Químicas. Universidad Complutense de Madrid, Ciudad Universitaria, 28040 Madrid, Spain

Supporting Information

ABSTRACT: An isomorphous series of five metal−organic frameworks of formula $[Ni_4(O_2CR)(OH)_2(4\text{-pyc})_5]$ [4-pyc = 4-pyridinecarboxylate or isonicotinate; R = C_6H_5 (**1**), 4-OMe-C_6H_4 (**2**), 2,6-$(OMe)_2$-C_6H_3 (**3**), 3,5-$(OMe)_2$-C_6H_3 (**4**), 3,4,5-$(OMe)_3$-C_6H_2 (**5**)] were obtained by solvothermal reactions. These compounds display a three-dimensional framework where the nickel atoms are coordinated to the hydroxyde anions and two different organic ligands: isonicotinate and phenylcarboxylate. Both hydroxyde (μ_3-OH) and phenylcarboxylate (μ_3-1κO,2κO,3$\kappa O'$) ligands are coordinated to nickel atoms of the same secondary building unit (SBU). The SBU consists of four edge-sharing NiA_6 octahedra (A = O, N). The isonicotinate ligands, however, act as linkers between SBUs displaying three different coordination modes: μ-1κN,2κO; μ_3-1κN,2κO,3$\kappa O'$; and μ_4-1κN,2:3$\kappa^2 O$,4$\kappa O'$. Nitrogen adsorption measurements were done to obtain textural parameters of these microporous networks. Micropore size distributions indicate cylindrical pores with diameters of approximately 0.80 nm. The values of Brunauer−Emmett−Teller surface areas (S_{BET}) obtained are in the range of 382−488 m^2/g, and the micropore volumes are between 0.13 cm^3/g and 0.19 cm^3/g. Both parameters are influenced by the substitution grade and position of the methoxy groups of the phenylcarboxylate ligand. The magnetic properties, which also depend on the arylcarboxylate ligands, vary from compound **1** (with only antiferromagnetic interactions) to compound **5**, which shows a spin glass behavior (T_g = 15 K).

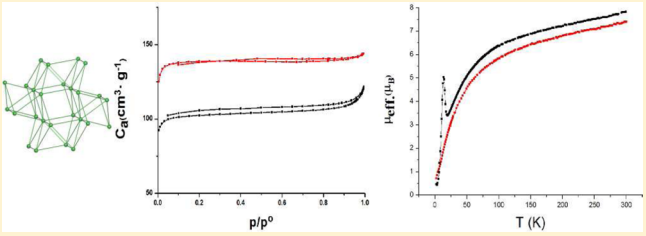

INTRODUCTION

Metal−organic frameworks (MOFs), also called porous coordination polymers (PCPs), are promising materials in several fields such as gas capture/storage, separation, ion exchange, and catalysis, and they also show interesting electric, luminescent, and optical properties.[1,2] Polyfunctional materials such as porous magnets are of particular interest for the design of magnetic sensors, low density magnets, and air magnetic separators. However, the construction of a porous ferromagnetic MOF constitutes a huge challenge: porosity requires long connectors, whereas magnetic ordering is favored with short distances between metal centers.[3] Nevertheless, MOFs show significantly better tunability of their structures than other well-known porous solids (e.g., zeolites). A careful choice of metal nodes and linkers would help define the framework, including its shape and the dimensions of the pores.[2]

There is a wealth of organic ligands to be used as connectors between many transition metals and rare-earths with different coordination numbers and geometries. Thus, the idea to construct porous structures using some specific building fragments has fascinated many researchers. In particular, numerous MOFs based on carboxylate ligands have been described[3] showing a remarkably high surface area and uniform pore size distribution. Another related strategy to prepare rigid three-dimensional structures is the use of carboxylate ligands with one additional donor atom of a different nature, which gives a high versatility for binding a great variety of transition metals. The isonicotinate ligand (4-pyridinecarboxylate, 4-pyc) presents a stable and rigid structure and is very adequate to prepare ordered coordination polymers with specific topologies.[4] Following our previous works in nickel MOFs with N- and O-donor ligands,[5,6] in this study we have used 4-pyridinecarboxylate and phenylcarboxylate ligands in order to produce a series of new three-dimensional MOFs, containing Ni(II) as magnetic centers and the substituted phenylcarboxylate ligands RCO_2^- [R = $(MeO)_mC_6H_{5-m}$, m = 0−3] as variable fragments. As a consequence, we are able to evaluate the influence of the substituents in the phenyl ring on the adsorption and magnetic properties within a series of isomorphous compounds of formula $[Ni_4(O_2CR)(OH)_2(4\text{-pyc})_5]$ [R = C_6H_5 (**1**), 4-OMe-C_6H_4 (**2**), 2,6-$(OMe)_2$-C_6H_3 (**3**), 3,5-$(OMe)_2$-C_6H_3 (**4**), 3,4,5-$(OMe)_3$-C_6H_2 (**5**)].

EXPERIMENTAL SECTION

General Comments and Physical Measurements. Reactants and solvents were used as received. Solvothermal syntheses were

Received: October 25, 2013
Revised: November 26, 2013
Published: December 6, 2013

   dx.doi.org/10.1021/cg401590w | Cryst. Growth Des. 2014, 14, 716−722

carried out in a Memmert Universal Oven UFE 400 with Teflon-lined stainless steel autoclaves. Microwave-assisted solvothermal reactions were carried out in an ETHOS One microwave oven using TFM Teflon closed vessels equipped with a temperature sensor and pressure controller. FT-IR spectra were recorded with a Perkin-Elmer Spectrum 100 with a universal ATR accessory with a spectral range of 4000−650 cm^{-1}. Elemental analyses were done by the Microanalytical Service of the Universidad Complutense of Madrid. Thermogravimetric analyses were performed in nitrogen atmosphere, up to 1000 °C, with a heating rate of 5 °C·min^{-1} with a Perkin-Elmer Pyris 1 TGA Instrument. The samples were also characterized by N_2 adsorption at 77 K. The adsorption−desorption measurements were made with ASAP 2020 equipment from Micromeritics. Prior to the experiments, the samples were outgassed at 423 K for 12 h. The isotherms were analyzed using the BET model with 0.162 nm^2 as the molecular cross-sectional area for adsorbed nitrogen.[7] Micropore size distributions were obtained by the Horvath−Kawazoe method[8] with the assumption of cylindrical pores.[9] Variable-temperature magnetic susceptibility data were measured with a Quantum Design MPMSXL superconducting quantum interference device (SQUID) susceptometer over a temperature range of 2−300 K. All data were corrected for the diamagnetic contribution of both the sample holder and the compound to the susceptibility. Molar diamagnetic corrections for the complexes were calculated on the basis of Pascal's constants.

Synthesis. General Procedure. A mixture of $Ni(NO_3)_2{\cdot}6H_2O$ (0.8 mmol, 0.24 g), the corresponding carboxylic acid (4.0 mmol), 4-cyanopiridine (1.0 mmol, 0.10 g), THF (9 mL), and water (3 mL) was sealed into a Teflon-lined stainless autoclave. The system was heated at 180 °C for 3 days under autogenous pressure and cooled slowly afterward. The green single crystals obtained were hand-picked, washed with ethanol (2 × 5 mL) and diethyl ether (5 mL), and dried in an oven at 100 °C. Finally, the crystals were allowed to hydrate with the moisture of the atmosphere for two weeks until a constant weight was reached. These samples were used simultaneously for elemental analyses and magnetic and TG measurements to minimize the influence of the variability of the number of solvent molecules located in the channels. Yields, elemental analyses, and IR absorptions are collected in Table S1 in the Supporting Information, and infrared spectra are shown in section S2.

Structural Analysis. Suitable crystals of compounds **1**−**5** were selected and mounted on a Bruker-Siemens Smart CCD diffractometer equipped with a normal focus 2.4 sealed tube X-ray source (Mo Kα radiation, λ = 0.71073 Å). More detailed information from data collection and structure refinement data is shown in Table S3 in the Supporting Information. Powder X-ray diffraction (PXRD) measurements were done on an X'Pert PRO ALPHA1 diffractometer with $\theta/2\theta$ configuration in samples retrieved after the sorption measurements to confirm that the initial structure (observed by single crystal X-ray diffraction) was maintained. The samples were kept in an oven at 100 °C before doing the PXRD measurements. Rietveld refinements were carried out using X'pert High Score Plus software in automatic mode (see section S4 in the Supporting Information).

RESULTS AND DISCUSSION

Synthesis of the Compounds. Numerous attempts were made to optimize the synthetic procedure to obtain the polymeric compounds $[Ni_4(O_2CR)(OH)_2(4\text{-pyc})_5]$ [4-pyc = 4-pyridinecarboxylate or isonicotinate; R = C_6H_5 (**1**), 4-OMe-C_6H_4 (**2**), 2,6-$(OMe)_2$-C_6H_3 (**3**), 3,5-$(OMe)_2$-C_6H_3 (**4**), 3,4,5-$(OMe)_3$-C_6H_2 (**5**)]. It was necessary to select an adequate procedure and suitable starting materials and to force the reaction conditions in order to avoid the formation of other isonicotinate compounds such as $[Ni_5(OH_2)_3(4\text{-pyc})_{10}]$ and, especially, the very stable compound $[Ni(OH_2)_4(4\text{-pyc})_2]$.[6,10] In the Experimental Section, only the best procedure found to isolate the complexes is described.

Following an approach similar to the one employed for other coordination complexes,[6,11] three different activation procedures were assayed: (a) refluxing solvent; (b) conventional solvothermal conditions; and (c) solvothermal microwave assisted. Only mixtures of unidentified insoluble compounds were obtained under refluxing solvents. Although microwave-assisted synthesis produced microcrystalline solids from compounds **1**−**5**, they were not easily separable from the insoluble impurities. In contrast, easily isolable large crystals were formed from conventional solvothermal synthesis. The yields shown in Table S1 were calculated by considering only the largest crystals in order to guarantee the purity of the samples.

The use of $NiCl_2{\cdot}6H_2O$, isonicotinic acid, relatively low temperatures or short times of reaction favors the formation of $[Ni(OH_2)_4(4\text{-pyc})_2]$.[6,10] The best reaction conditions to isolate compounds **1**−**5** were found to be using $Ni(NO_3)_2{\cdot}6H_2O$ as the Ni source, a large excess of the benzoic acid $[(MeO)_mC_6H_{5-m}CO_2H$, m = 0−3], 4-cyanopyridine instead of isonicotinic acid, high temperatures, and long reaction times (although reaction times longer than 3 days did not improve the yield). It is well-known that 4-cyanopyridine easily undergoes a hydrolysis process to yield 4-pyridinecarboxylate (4-pyc) in solvothermal conditions.[12] Nickel(II) hydroxide was also used to prepare compounds **1**−**5**, and in that case, a small impurity of $Ni(OH)_2$ together with the previously reported MOF $[Ni_5(OH_2)_3(4\text{-pyc})_{10}]$[6] was also found.

Infrared. All of the infrared spectra show intense bands of the ν_a(COO) and ν_s(COO) modes in the 1610−1604 cm^{-1} and 1405−1371 cm^{-1} regions. The energy difference between both stretching vibrations, ν_a(COO) and ν_s(COO), depends on the coordination mode of the carboxylate group. The highest differences between those values are reported for unidentate carboxylates, whereas lower values are expected for bridging modes.[6,13] Differences of 226−231 cm^{-1} and 199−206 cm^{-1} were found in compounds **1**−**5**, which were assigned to unidentate and bridging modes, respectively.

More detailed information from the infrared spectra and assignment of the bands of all compounds is shown in section S2 in the Supporting Information.

Thermal Stability. The thermogravimetric weight loss of all of the compounds displays a two-step decomposition process. The first weight loss takes place from room temperature to approximately 80 °C. It corresponds to the loss of the solvent molecules, which are located in the cavities in the solid (see below crystal structure descriptions). The framework is stable up to a temperature around 300 °C, when the second weight loss occurs to form nickel(II) oxide.

As an example, the thermogravimetric curve of compound **3** is shown in Figure 1. The curves obtained for compounds **1**, **2**, **4**, and **5** and a table with more detailed information are included in section S5 in the Supporting Information.

Description of the Structures. The five compounds presented here display a three-dimensional framework with formula $[Ni_4(OC_2R)(OH)_2(4\text{-pyc})_5]_n$ where R = $(MeO)_mC_6H_{5-m}$. In this coordination polymeric structure, the hydroxyde anions and two different organic ligands, isonicotinate and phenylcarboxylate, are coordinated to the nickel atoms. Compounds **1**−**5** constitute an isomorphous series of three-dimensional MOFs containing a tetranickel secondary building unit (SBU). This SBU displays 10 points of extension and consists of four edge-sharing NiA_6 octahedra (A = O, N). A simplified picture of the SBU core and the polyhedra representation of the SBU with the extension points are shown in Figures 2 and 3, respectively. This framework is

dx.doi.org/10.1021/cg401590w | Cryst. Growth Des. 2014, 14, 716−722

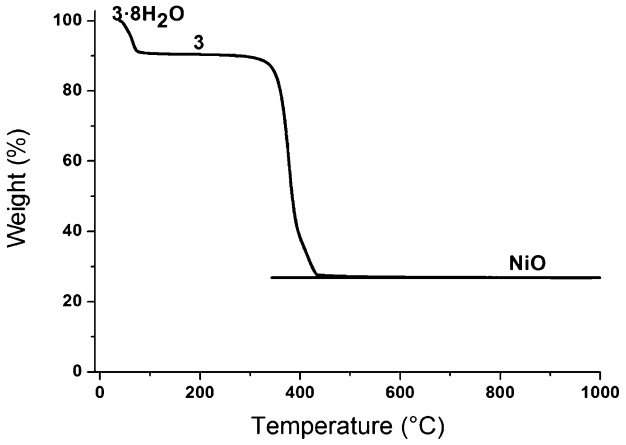

Figure 1. Thermogravimetric weight loss curve for **3**.

analogous to the one described by Chen et al., obtained using an aliphatic carboxylic acid.[14]

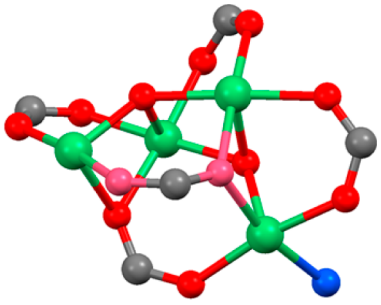

Figure 2. View of the tetranickel cluster core. Rings in the aromatic ligands have been omitted for clarity. The oxygen atoms from the phenylcarboxylate ligands are depicted in pink.

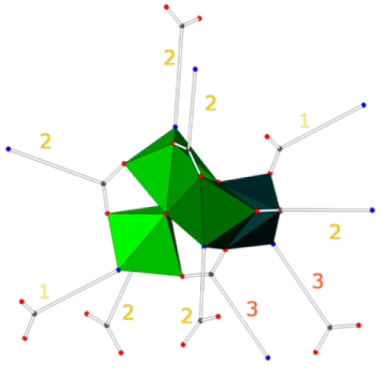

Figure 3. Tetranickel SBU with the extension points. For simplicity, isonicotinate ligands are displayed as solid lines with N atoms in blue and O atoms in red. The labels represent the coordination mode of the isonicotinate ligands, according to Figure 4.

Regarding the ligands, both hydroxyde (μ_3-OH) and phenylcarboxylate (μ_3-1κO,2κO,3$\kappa O'$) moieties are coordinated to nickel atoms from the same SBU, and therefore they do not act as linkers between metal clusters. The isonicotinate ligands, however, link different SBUs, displaying three coordination modes: μ-1κN,2κO; μ_3-1κN,2κO,3$\kappa O'$, and μ_4-1κN,2:3$\kappa^2 O$,4$\kappa O'$ (Figure 4). Each SBU is connected to nine adjacent units by 10 isonicotinate ligands (Figure 5). The distances between clusters in the series range from ~10.6 Å (the shortest ones) to ~13.1 Å (the longest ones), and they are not related to the number or

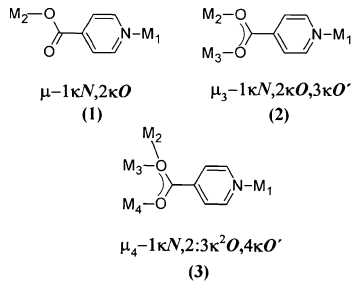

Figure 4. Coordination modes presented by the isonicotinate ligand found in the present work.

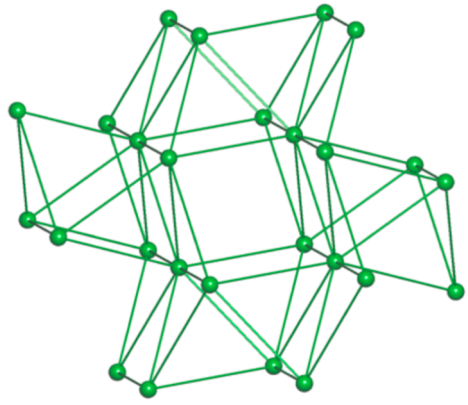

Figure 5. Representation of the uninodal **vna** 9-connected underlying net.

position of the substituents in the aromatic rings (see Table S3a in the Supporting Information).

The disposition of the SBUs gives rise to a porous structure with square and triangular channels parallel to the *a* axis (Figure 6). The aromatic rings of the phenylcarboxylate ligands are located inside the square channels, with the rings from the phenylcarboxylate ligands adopting a different position depending on the number of methoxy substituents. However, these rings are not attached to the framework by strong bonds and

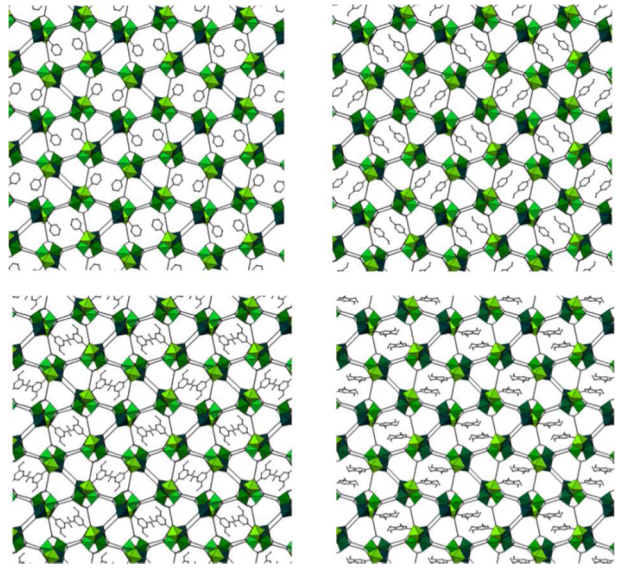

Figure 6. View along the *a* axis of the channels present in the structure of **1** (top, left), **2** (top, right), **4** (bottom, left), and **5** (bottom, right).

dx.doi.org/10.1021/cg401590w | *Cryst. Growth Des.* 2014, 14, 716−722

Table 1. Crystal Data for 1−5

	1	2	3	4	5
chemical formula	$C_{37}H_{27}N_5Ni_4O_{14}$	$C_{38}H_{29}N_5Ni_4O_{15}$	$C_{39}H_{31}N_5Ni_4O_{16}$	$C_{39}H_{31}N_5Ni_4O_{16}$ 0.5H_2O·0.5THF	$C_{40}H_{33}N_5Ni_4O_{17}$
formula weight	1000.48	1030.50	1060.53	1104.58	1090.55
crystal system	monoclinic	monoclinic	monoclinic	monoclinic	monoclinic
space group	$P2_1/n$	$P2_1/n$	$P2_1/n$	$P2_1/n$	$P2_1/n$
a (Å)	13.1181(8)	13.029(1)	13.2430(6)	13.131(1)	13.053(1)
b (Å)	18.340(1)	18.553(1)	18.2511(8)	18.385(1)	18.557(1)
c (Å)	21.561(1)	22.002(2)	21.897(1)	21.734(2)	22.114(1)
β (deg)	101.558(1)	102.837(2)	104.174(1)	101.981(2)	103.263(1)
V (Å^3)	5082.1(5)	5185.7(7)	5131.4(4)	5132.5(7)	5213.8(7)
Z	4	4	4	4	4
D_{calcd} (g cm^{-3})	1.308	1.320	1.373	1.429	1.389
μ (mm^{-1})	1.517	1.490	1.510	1.514	1.489
reflections measured	39623	39678	40059	37795	38341
unique reflections	9281	9211	9389	9397	9553
R_{int}	0.0699	0.1386	0.0455	0.0834	0.1076
transmission range	0.8631−0.6424	0.8776−0.5112	0.8279−0.6125	0.8048−0.6194	0.8902−0.796
refined parameters	529	562	579	617	586
R (F, $F^2 > 2\sigma$)	0.0576	0.0824	0.0531	0.0684	0.0880
R_w (F^2, all data)	0.2113	0.3001	0.2049	0.2211	0.3078
GOF (F^2, all data)	1.012	1.015	1.037	1.047	1.021

have a large degree of freedom. This fact can be seen in the disorder displayed by this part of the structure in all of the compounds, especially in **4** and **5**. Interestingly, there is no head−tail disorder in the μ-1κN,2κO isonicotinate ligands, in contrast to the situation found previously in other related nickel isonicotinate MOFs.[6,14] However, one of the members in the series (**2**) presents this ligand in the opposite configuration as the rest of the isostructural compounds here described.

Considering the tetranickel clusters as nodes and the isonicotinate ligands as linkers, the framework presents a **vna** 9-connected uninodal 3D net[15] (Figure 5). The underlying net possesses a high degree of connectivity, which is not unusual when polymetallic SBUs are considered as nodes. This is because a SBU can display more points of extension than a monometallic unit, especially in the case of transition metals, as the extension points in the case of monometallic nodes are restricted to the coordination number of the metal centers.

The number and disposition of the substituents on the phenyl ring do not have a crucial influence on the dimensions of the cell parameters, as the channels where they are located are large enough to accommodate any of them. However, there is a slight increment in the cell volume when the value of m increases, although the effect of the *para* substituent for the MOFs with m = 1 or 3 seems to be more important than the increase in the number of methoxy groups (Table 1).

In contrast, the presence of a group linked to the carboxylate with enough steric volume seems to be a requisite for the formation of this structural type. Indeed, the same structural type is found when the aliphatic carboxylic acid $EtCO_2H$ is used, although the reaction conditions were different.[14] We assayed to synthesize an analogous compound with $MeCO_2H$, and our attempts were unsuccessful. This substituent, which does not play a role in the connectivity between SBUs, could have an important templating effect in the formation of some of the channels and the structural stability when the compounds undergo desolvation processes.

As the size and shape of the substituent do not have a proportional effect on the dimensions of the channels, the driving force behind the formation of these channels and the porosity of the solid structure is probably the existence of weak interactions between the solvent molecules and these groups. The solvent molecules can easily be removed afterward, leaving the channels empty to accommodate other molecules such as N_2 or H_2. The stability of the framework is not affected, as proven by the thermogravimetric and PXRD studies, measured after the N_2 sorption measurements (see S4 in the Supporting Information). Thus, the PXRD diffractograms simulated from the X-ray single crystal determination and the PXRD measurements carried out after the N_2 sorption agree well. However, little differences have been observed in some cases. These differences could be due to two facts: (a) the PXRD experiments could not be made in anhydrous conditions, and some water molecules can be incorporated in the channels; and (b) some small variations in the framework could also happen as a consequence of the sorption process (*breathing* of the framework), and this distortion could contribute to worsen the fit between the experimental and theoretical data.

Adsorption Properties. Textural parameters were obtained from crushed single crystals of all the complexes. The nitrogen adsorption isotherms measured at 77 K show a Type I character, as expected due to the microporous structure of these materials. The amount of nitrogen uptake increases abruptly at low pressures and reaches plateaus of 137, 127, 124, 110, and 101 cm^3(SPT)g^{-1} at p/p^0 values of 0.1 for **1**−**5**, respectively (Figure 7). The small hysteresis loops observed can be explained by the existence of a narrowing of the channels, which causes a slight difference between adsorption and desorption processes.

The values of surface areas were obtained by the BET (S_{BET}) and Langmuir ($S_{Langmuir}$) equations using the adsorption branch of the isotherms (section S6 in the Supporting Information and Table 2).

Liquid micropore volumes (V_{mp}) and micropore size distributions were calculated by the Horvath−Kawazoe method[8] considering cylindrical pores (Table 2). The micropore size distributions show two maxima in the micropore diameter (D_{mp}) around 0.80 nm in all of the compounds. As an example, the micropore volume and the microporore size

dx.doi.org/10.1021/cg401590w | *Cryst. Growth Des.* 2014, 14, 716−722

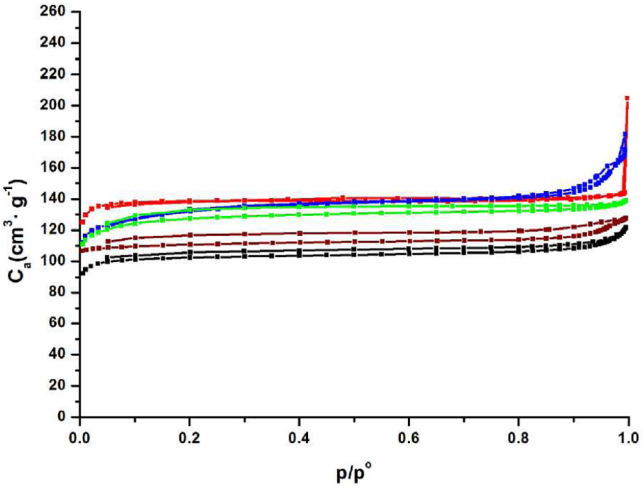

Figure 7. Adsorption−desorption isotherms for **1** (red), **2** (blue), **3** (green), **4** (brown), and **5** (black).

Table 2. Textural Parameters for 1−5

	1	2	3	4	5
S_{BET} (m^2/g)	488	469	477	390	382
$S_{Langmuir}$ (m^2/g)	491	467	490	393	373
D_{mp} (nm)	0.80	0.78	0.80	0.82	0.78
	0.82	0.82	0.81	0.83	0.80
V_{mp} (cm^3/g)	0.18	0.19	0.18	0.14	0.13
V_{mp}^{cryP} (cm^3/g)[a]	0.26	0.26	0.22	0.19	0.20
V_{mp}^{cryM} (cm^3/g)[b]	0.20	0.21	0.17	0.13	0.14

[a]Calculated using PLATON.[16] [b]Calculated with Mercury Voids[17] (Contact Surface; Probe Radius: 1.7 Å).

distribution for **1** are shown in Figure 8. The rest of the measurements are shown in section S6 in the Supporting Information.

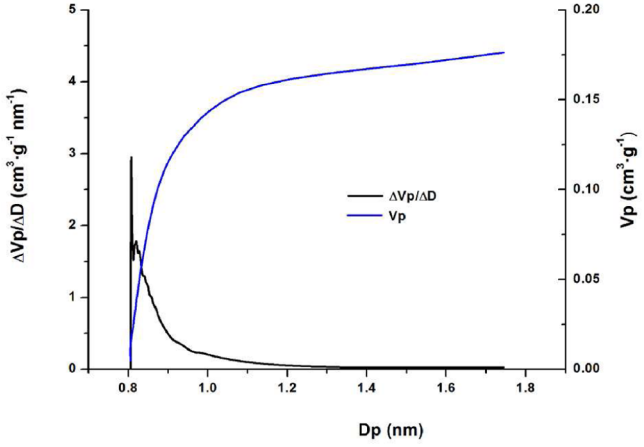

Figure 8. Micropore volume and micropore size distribution for **1**.

Taking into account the value of 0.162 nm^2 for the cross-sectional area of the nitrogen molecules and the volume of gas adsorbed in the micropores measurements [114 (**1**), 110 (**2**), 116 (**3**), 90 (**4**), and 86 (**5**) cm^3(SPT)g^{-1}], the surface areas were also estimated using the equation shown in S6j (Supporting Information). Thus, the obtained values were 496 (**1**), 479 (**2**), 505 (**3**), 392 (**4**), and 374 (**5**) m^2·g^{-1}, which are close to those obtained with the BET and the Langmuir fittings.

It is known that the Langmuir theory assumes single layer adsorption and leads to larger specific surfaces areas compared to the BET theory in multilayer processes. However, since the channel diameters in compounds **1**−**5** are around 0.80 nm, only one single layer can be accommodated in each wall in the micropore filling (nitrogen diameter = 0.35 nm), and BET and Langmuir models must give similar values.

Theoretical liquid pore volumes were calculated using PLATON[16] (V_{mp}^{cryP}) and Mercury Voids[17] (V_{mp}^{cryM}) software obtaining a good and an excellent agreement, respectively, with the experimental data (Table 2).

There is a significant difference between surface areas and micropore volumes of complexes with none (**1**) or one methoxy group (**2**), compared to the compound in which the carboxylate ligand has three methoxy substituents (**5**). The complexes with dimethoxyphenylcarboxylate ligands display different values of these parameters depending on the position of the methoxy groups. Thus, the nitrogen uptake of 2,6-dimethoxyphenylcarboxylato compound (**3**) is similar to that measured for **1** and **2**. However, the gas adsorption of the 3,5-dimethoxy derivative (**4**) is similar to that found for **5**. Therefore, it seems that the adsorption is specially obstructed by the methoxy groups situated in the *meta* disposition.

Although the measured surface areas of **1**−**5** are not especially high,[18] they are similar to those reported for other porous magnets.[3,14]

Magnetic Properties. The magnetic data were determined on polycrystalline samples obtained from crushed single crystals. The solvent molecules deduced from the elemental analyses were considered in the molar weight employed in these studies.

Magnetic moments at room temperature, measured at 0.5 T, for **1**−**5** are 6.21, 6.20, 5.69, 5.86, and 6.35 μ_B, respectively, which are close to the expected value for four magnetically isolated Ni(II) ions (Figure 9, top). The magnetic moment versus temperature representations show a continuous decrease as the temperature decreases. This behavior indicates predominant antiferromagnetic interactions. The magnetic susceptibility of compounds **1**, **3**, and **4** shows a continuous increase when the temperature decreases, until a broad maximum is reached at around 35 K. From this point on, the susceptibility decreases down to 5−6 K. For compound **5**, a maximum is reached at 17 K, although a shoulder is observed at 35 K. The susceptibility curve of compound **2** shows two shoulders at 35 and 15 K approximately. The magnetic susceptibility vs temperature curves measured at 0.5 T for all the complexes are shown in section S7 in the Supporting Information.

Magnetization measurements vs magnetic field reveal the existence of a small hysteresis loop for **2** (section S7 in the Supporting Information) and **5** (Figure 10). To further investigate the magnetic behavior, a lower magnetic field (0.01 T) was employed (Figure 9, bottom). The magnetic moment vs temperature curve (0.01 T) presents a maximum at 13−14 K for **2** and **5**, and a shoulder for **3** and **4**. An additional maximum is observed at 6 K in the curve of **2**. These behaviors are very similar to those found in $[Ni_4(O_2CEt)(OH)_2(4\text{-pyc})_5]\cdot 6EtOH\cdot 2H_2O$ and $[Co_4(EtOH)(OH)_2(OH_2)(4\text{-pyc})_5](NO_3)\cdot 2EtOH\cdot 4H_2O$, respectively,[14] and also in the tricobalt MCF-39 compound.[19] For the three compounds, the presence of spin glass behavior was claimed. Interestingly, a gradual

dx.doi.org/10.1021/cg401590w | Cryst. Growth Des. 2014, 14, 716−722

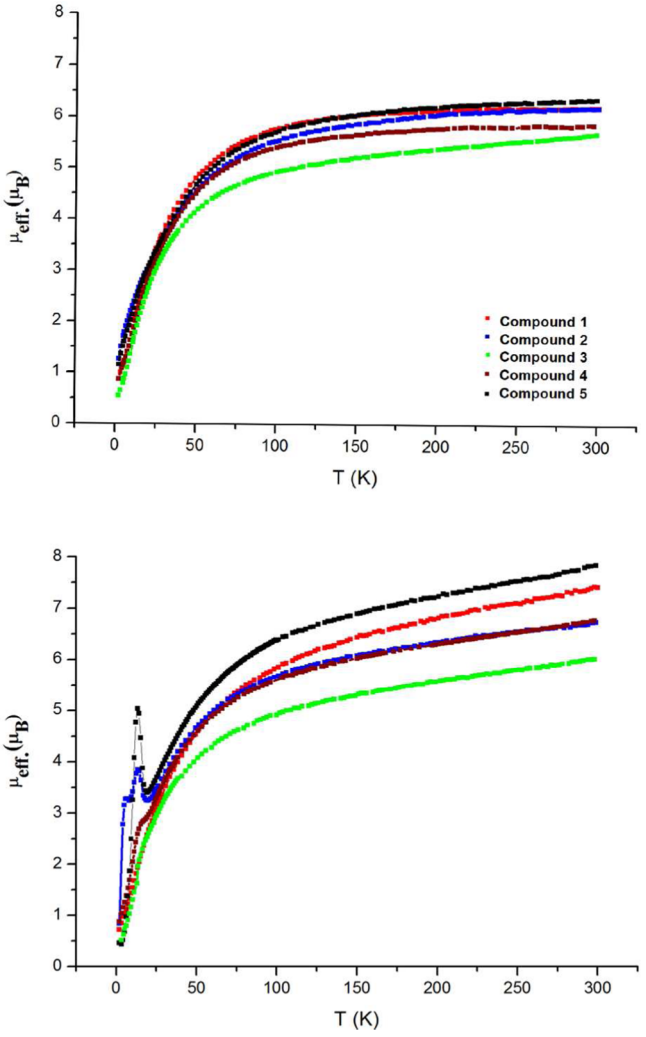

Figure 9. Magnetic moments vs temperature for **1**−**5** measured at 0.5 T (top) and 0.01 T (bottom).

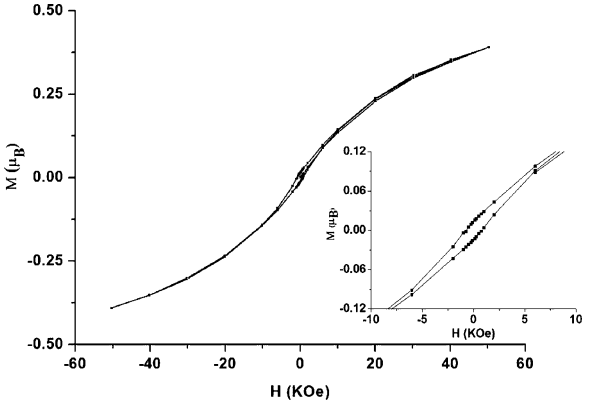

Figure 10. Magnetization vs magnetic field measured at 2 K for **5**. Inset: Low field region.

variation of this phenomenon is observed in the series in the order **1**, **3**, **4**, **2**, and **5**.

The magnetic susceptibility vs temperature curve measured at 0.01 T presents at 12−14 K a maximum for compounds **2**−**5** (S7 in the Supporting Information). The curve of compound **2** also shows a second maximum at 5 K.

A phase transition is suggested by the divergences observed in the field-cooled (FC) and zero-field-cooled (ZFC) magnetization measurements performed for **2**−**5** at 14−18 K (Figure 11 and section S7 in the Supporting Information).

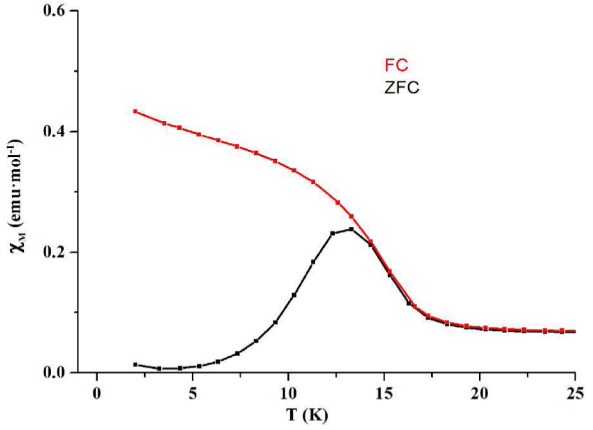

Figure 11. Field-cooled and zero-field-cooled magnetization for **5**.

The *ac* magnetic measurements for **2** and **5** show a moderately frequency-dependent peak around 14 K (section S7 in the Supporting Information and Figure 12). The

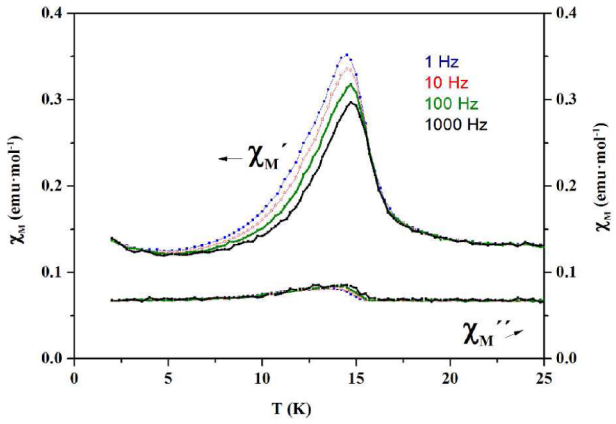

Figure 12. Magnetic susceptibility vs temperature in an *ac* measurement of **5**.

quantification of this frequency-dependence can be evaluated by the equation $\phi = \Delta T_p/[T_p \Delta(\log f)]$ (T_p = peak temperature; f = frequency). The ϕ values obtained are 0.014 and 0.007 for **2** and **5**, respectively. These values are typical for a spin glass behavior.[20]

We have carefully analyzed the slight differences in the cell parameters and the intra- and intercluster Ni−Ni distances, and we have not found any correlation between them and the gradual variation of the magnetic properties. This variation should then be related to the number and disposition of the methoxy groups in the arylcarboxylate ligand, which is the most significant difference in these isostructural compounds. Specifically, a slight increase of the basicity of the ligand could increase the ferromagnetic interactions. The basicity of these ligands depends on the electron density on the C_{ipso} of the arylcarboxylate and on the dihedral angle between the aromatic ring and the CO_2 plane. The aromatic carboxylate is not activated in **1**, which means that this compound is the less

dx.doi.org/10.1021/cg401590w | Cryst. Growth Des. 2014, 14, 716−722

basic. In contrast, compound **3** contains the most activated C_{ipso}. However, the dihedral angle is very large (54.92°), which barely allows electronic communication between the ring and the carboxylate group. The electron density of the C_{ipso} in **4** is low despite the fact that the ring is rather activated. Finally, compounds **2** and **5** display electron rich C_{ipso} and low dihedral angles.

CONCLUSIONS

The number and position of the methoxy groups in the phenylcarboxylate ligands, which are located inside the channels of the MOFs in this isostructural series of compounds, clearly affect the nitrogen adsorption. This adsorption is higher in compounds **1**, **2**, and **3**, in which either the number of methoxy group is lower or they are situated in the *ortho* position. More surprising is how subtle differences far from the metal centers can affect the magnetic behavior of the compounds. Although antiferromagnetic interactions are present in all of the compounds, the maximum of the magnetic moment and the susceptibility values around 14 K rises progressively from **1** to **5** due to a spin glass behavior.

ASSOCIATED CONTENT

Supporting Information

Yields, elemental analyses, and IR absorptions for compounds of the formula $[Ni_4(O_2CR)(OH)_2(4\text{-pyc})_5]\cdot nH_2O$. Infrared spectra, single crystal experimental data, powder X-ray diffractograms, thermogravimetric weigh loss curves, adsorption measurements, additional magnetic data, and X-ray crystallographic files (CIFs). This material is available free of charge via the Internet at http://pubs.acs.org. CCDC-968492−968496 contains the supplementary crystallographic data for this paper. These data can be obtained free of charge from The Cambridge Crystallographic Data Centre via www.ccdc.cam.ac.uk/data_request/cif.

AUTHOR INFORMATION

Corresponding Authors

*E-mail: sherrero@quim.ucm.es (S.H.).
*E-mail: reyesja@quim.ucm.es (R.J.-A.).

Notes

The authors declare no competing financial interest.

ACKNOWLEDGMENTS

Financial support received from the Spanish Ministerio de Economía y Competitividad (CTQ2011-23066) and Comunidad de Madrid (S2009/MAT-1467) is gratefully acknowledged.

REFERENCES

(1) (a) Zhou, H.-C.; Long, J. R; Yaghi, O. M. *Chem. Rev.* **2012**, *112*, 673−1268. (Metal−organic frameworks issue). (b) Long, J. R; Yaghi, O. M. *Chem. Soc. Rev.* **2009**, *38*, 1201−1508 (Metal−organic frameworks issue).

(2) (a) Stock, N.; Biswas, S. *Chem. Rev.* **2012**, *112*, 933−969. (b) Gu, Z.-Y.; Yang, C.-X.; Chang, N.; Yan, X.-P. *Acc. Chem. Res.* **2012**, *45*, 734−745. (c) Champness, N. R. *Dalton Trans.* **2011**, *40*, 10311−10315. (d) Farrusseng, D.; Aguado, S.; Pinel, C. *Angew. Chem., Int. Ed.* **2009**, *48*, 7502−7513.

(3) (a) Dechambenoit, P.; Long, J. R. *Chem. Soc. Rev.* **2011**, *40*, 3249−3265. (b) Kurmoo, M. *Chem. Soc. Rev.* **2009**, *38*, 1353−1379. (c) Maspoch, D.; Ruiz-Molina, D.; Veciana, J. *J. Mater. Chem.* **2004**, *14*, 2713−2723.

(4) (a) Liu, T.; Luo, D.; Xu, D.; Zenga, H.; Lin, Z. *Dalton Trans.* **2013**, *42*, 368−371. (b) Jiang, G.; Wu, T.; Zheng, S.-T.; Zhao, X.; Lin, Q.; Bu, X.; Feng, P. *Cryst. Growth Des.* **2011**, *11*, 3713−3716. (c) Clemente-León, M.; Coronado, E.; Martí-Gastaldo, C.; Romero, F. M. *Chem. Soc. Rev.* **2011**, *40*, 473−497.

(5) (a) Cortijo, M.; González-Prieto, R.; Herrero, S.; Jiménez-Aparicio, R.; Sánchez-Rivera, P. *Eur. J. Inorg. Chem.* **2013**, 5523−5527. (b) Cortijo, M.; Herrero, S.; Jiménez-Aparicio, R.; Matesanz, M. *Inorg. Chem.* **2013**, *52*, 7087−7093.

(6) Cortijo, M.; Herrero, S.; Jiménez-Aparicio, R.; Perles, J.; Priego, J. L.; Torralvo, M. J.; Torroba, J. *Eur. J. Inorg. Chem.* **2013**, 2580−2590.

(7) Rouquerol, F.; Rouquerol, J.; Sing, K. *Adsorption by Powders and Porous Solids, Principles, Methodology and Applications*, Academic Press: New York, 1999; p 171.

(8) Rege, S. U.; Yang, R. T. *AIChE J.* **2000**, *46*, 734−750.

(9) Barret, E. P.; Joyner, L. G.; Halenda, P. P. *J. Am. Chem. Soc.* **1951**, *73*, 373−380.

(10) (a) Ma, T.-H.; Yu, J.-H.; Ye, L.; Xu, J.-Q.; Wang, T.-G.; Lü, C.-H. *J. Mol. Struct.* **2003**, *654*, 47−53. (b) Batten, S. R.; Harris, A. R. *Acta Crystallogr.* **2001**, *E57*, m7−m8.

(11) (a) Delgado, P.; González-Prieto, R.; Jiménez-Aparicio, R.; Perles, J.; Priego, J. L.; Torres, M. R. *Dalton Trans.* **2012**, *41*, 11866−11874. (b) Herrero, S.; Jiménez-Aparicio, R.; Perles, J.; Priego, J. L.; Saguar, S.; Urbanos, F. A. *Green Chem.* **2011**, *13*, 1885−1890. (c) Herrero, S.; Jiménez-Aparicio, R.; Perles, J.; Priego, J. L.; Urbanos, F. A. *Green Chem.* **2010**, *12*, 965−967.

(12) (a) Pluchery, O.; Climent, V.; Rodes, A.; Tadjeddine, A. *Electrochim. Acta* **2001**, *46*, 4319−4329. (b) Evans, O. R.; Wang, Z.; Xiang, R. G.; Foxman, B. M.; Lin, W. *Inorg. Chem.* **1999**, *38*, 2969−2973. (c) Mathew, C. D.; Nagasawa, T.; Kobayashi, M.; Yamada, H. *Appl. Environ. Microbiol.* **1988**, *54*, 1030−1032.

(13) Nakamoto, K. *Infrared and Raman Spectra of Inorganic and Coordination Compounds, Part B, Applications in Coordination, Organometallic and Bioinorganic Chemistry*, 6th ed.; Wiley: Hoboken, NJ, 2009.

(14) Chen, Q.; Xue, W.; Lin, J.-B.; Lin, R.-B.; Zeng, M.-H.; Chen, X.-M. *Dalton Trans.* **2012**, *41*, 4199−4206.

(15) Alexandrov, E. V.; Blatov, V. A.; Kochetkov, A. V.; Proserpio, D. M. *CrystEngComm* **2011**, *13*, 3947−3958.

(16) Spek, A. L. *PLATON, A Multipurpose Crystallographic Tool*; Utrech University: Utrecht, The Netherlands, 2001.

(17) *Mercury Voids*, version 3.0; *Cambridge Crystallographic Data Centre*; University Chemical Laboratory: Cambridge, U.K., 2012.

(18) Furukawa, H.; Ko, N.; Go, Y. B.; Aratani, N.; Choi, S. B.; Choi, E.; Yazaydin, A. O.; Snurr, R. Q.; O'Keeffe, M.; Kim, J.; Yaghi, O. M. *Science* **2010**, *329*, 424−428.

(19) Chen, Q.; Xue, W.; Wang, B.-Y.; Zeng, M.-H.; Chen, X.-M. *CrystEngComm* **2012**, *14*, 2009−2014.

(20) Mydosh, J. A. *Spin Glasses: An Experimental Introduction*; Taylor & Francis: London, 1993.